# Experimental and theoretical study of an atmospheric air plasma-jet

M. Xaubet, L. Giuliani, D. Grondona, and F. Minotti

Citation: Physics of Plasmas **24**, 013502 (2017); doi: 10.1063/1.4973555
View online: http://dx.doi.org/10.1063/1.4973555
View Table of Contents: http://aip.scitation.org/toc/php/24/1
Published by the American Institute of Physics

# Experimental and theoretical study of an atmospheric air plasma-jet

M. Xaubet,[1,2] L. Giuliani,[1,2] D. Grondona,[1,2] and F. Minotti[1,2]
[1]*Universidad de Buenos Aires, Facultad de Ciencias Exactas y Naturales, Departamento de Física, Buenos Aires, Argentina*
[2]*CONICET – Universidad de Buenos Aires, Instituto de Física del Plasma (INFIP), Buenos Aires, Argentina*

(Received 4 November 2016; accepted 19 December 2016; published online 4 January 2017)

In this work, we present an experimental and theoretical study of a low frequency, atmospheric plasma-jet discharge in air. Voltage-current characteristics and spectroscopic data were experimentally obtained, and a theoretical model developed to gain information of different aspects of the discharge. The discharge is modeled as a cathode layer with different mechanisms of electron emission and a main discharge channel that includes the most important kinetic reactions and species. From the electric measurements, it is determined that high electric field magnitudes are attained in the main channel, depending on the gas flow rate. Using the voltage-current characteristics as an input, the model allows to determine the plasma state in the discharge, including electron, gas, and molecular nitrogen vibrational temperatures. The model also allows to infer the mechanisms of secondary electron emission that sustain the discharge. *Published by AIP Publishing.* [http://dx.doi.org/10.1063/1.4973555]

## I. INTRODUCTION

Non-thermal, atmospheric-pressure plasma jets are a fundamental tool in a wide range of technological and bio-medical applications.[1–3] Important advantages of these devices are their relative simplicity, easy operation, power efficiency, and the variety of possible active species production depending on design, type of gas employed, etc.

In spite of their widespread use, still much effort is needed to fully understand the basic physical aspects of these devices, in particular, the mechanisms of generation and sustainment of the discharge, and the characteristics of the generated plasma and of the active species. These latter aspects are particularly complex for gases other than noble gases, and especially in the case of air. We have recently presented a study of a low-frequency plasma jet (without a dielectric barrier) operating with argon[4] and found that a rather involved model is required to properly account for the plasma discharge characteristics. It was found that the discharge consists of a non-thermal plasma with a current channel of submillimeter diameter and that impact on the cathode by metastable excited argon atoms, generated under the action of the relatively high electric field in the cathode layer, are required to produce the flow of secondary electrons needed to sustain the discharge. Also, proper modeling and matching of the main discharge channel and cathode layer is required to correctly reproduce the measured voltage-current (V-I) characteristic and temperatures derived from spectroscopic data.

In the present work, we perform a similar analysis for the much more complex case of a plasma-jet operating with air. Using the general cathode layer model previously developed and a new model of the main discharge channel, whose input is the measured V-I characteristic, different aspects of the discharge can be explained. One of the most interesting results is the fact that the electric field in the discharge main channel attains higher values than in the similar air discharges, and that these values are up to some point controlled by the gas flow rate (the higher the flow rate the higher the electric field). These high fields produce energetic electrons that can be used, for instance, to affect chemical reactions having high energy thresholds. Another point is that as electron collisions readily excite vibrational levels of molecular nitrogen ($N_2$), which in turn transfer energy effectively to translational modes of the heavy species, the gas temperatures are high enough to allow field-enhanced thermionic emission by the cathode to be effective in the sustainment of the discharge.

## II. MODEL OF THE DISCHARGE

### A. Model of the cathode layer

The derivation and details of the cathode layer model can be seen in Ref. 4, of which we here give a short account.

The variables considered are the local electron number density $n_e$ and the axial electric field magnitude $E$, from which non-dimensional variables are defined as

$$\eta \equiv \frac{n_e}{n_\infty}, \quad \xi \equiv \frac{E_\infty}{E}, \tag{1}$$

where $n_\infty$ and $E_\infty$ are the corresponding variables at the main channel (for $n_e$ the average over the channel section is employed). From the continuity equations for electrons and ions, together with Poisson equation, a single differential equation is derived relating the variables defined by relations (1), given as

$$\frac{1}{\eta}\frac{d\eta}{d\xi} = \frac{1}{\xi} + \frac{\tilde{\alpha}}{\xi^2(\xi-\eta)} - \tilde{\beta}\frac{\eta + (\xi-\eta)\mu_e/\mu_i}{\xi(\xi-\eta)}, \tag{2}$$

where $\tilde{\alpha}$ and $\tilde{\beta}$ are dimensionless ionization and recombination coefficients, respectively, given by

$$\tilde{\alpha} \equiv \alpha L, \quad \tilde{\beta} \equiv \frac{\varepsilon_0}{\mu_e e}\beta, \tag{3}$$

where the constant $L$, with dimensions of length, is given by

$$L \equiv \frac{\varepsilon_0 E_\infty}{e n_\infty}\frac{\mu_i}{\mu_e}, \tag{4}$$

$e$ is the elementary charge, $\alpha$ is the Townsend's ionization coefficient, $\beta$ is the bulk recombination coefficient, and $\mu_{e,i}$ are the electron and ion mobilities.

The boundary conditions at the cathode result in

$$\frac{\eta_0}{\xi_0} = \frac{\gamma}{\gamma+1}\left[1 + \frac{\phi_0}{\gamma n_\infty \mu_e E_\infty}\right], \tag{5}$$

$$\eta_0 \tilde{\alpha}(\xi_0) = \xi_0(\xi_0 - \eta_0)(\xi_0 - \eta_0 + \tilde{\beta}\eta_0), \tag{6}$$

where $\xi_0$ and $\eta_0$ denote the values of $\xi$ and $\eta$, respectively, at the cathode, $\gamma$ is the secondary emission coefficient, and $\phi_0$ is the flow of electrons emitted from the cathode due to mechanisms other than secondary emission by ion impact.

Given a value of $\phi_0$, expressions (5) and (6) determine the values $\xi_0$ and $\eta_0$, allowing to integrate Eq. (2) up to $\xi = 1$, the value of the nondimensional variable at the channel. In this way, the voltage drop in the cathode layer $\Delta V$ and the cathode layer thickness $\Delta x$ are obtained as

$$\Delta V = E_\infty L \int_{\xi_0}^{1} \frac{d\xi}{\xi^3(\xi - \eta)} \tag{7}$$

and

$$\Delta x = L \int_{\xi_0}^{1} \frac{d\xi}{\xi^2(\xi - \eta)}, \tag{8}$$

respectively.

As models of $\phi_0$, we consider electron emission from the cathode by thermoionic effect, as well as by interaction with atoms or molecules excited at metastable levels.

For electric fields at the cathode surface below $5 \times 10^9$ V m$^{-1}$, the emitted electron flow (electrons per second per square meter) by the thermoionic–Schottky effect can be modeled as[5]

$$\phi_{TE} = \chi\, 1.35 \times 10^{33} T^2 \exp\left[-\frac{\varphi_m - V_E}{T}\right], \tag{9}$$

where $T$ is in eV units, $\varphi_m$ is the metal work function, and $V_E = \sqrt{eE_0/(4\pi\varepsilon_0)}$, with $E_0 = E_\infty/\xi_0$ the electric field at the cathode. The non-dimensional constant $\chi$ can take values approximately between 0.125 and 2.5 to account for different surface conditions.[6]

The flow of electrons emitted by the impact of metastable atoms is given as

$$\phi_m = \gamma_m n_\infty \mu_e E_\infty L \int_{\xi_0}^{1} \frac{\alpha_m(\xi)\eta}{\xi^3(\xi - \eta)} \exp[k_m x(\xi)] d\xi, \tag{10}$$

where $k_m = 1/\sqrt{D_m \tau_m}$, $\alpha_m$ is the Townsend's coefficient for atom excitation to the considered level, $\tau_m$ is the lifetime of excited atoms, and $D_m$ is their diffusion coefficient. The spatial variable $x(\xi)$ is obtained, from Eq. (8), by the integration of

$$\frac{dx}{d\xi} = \frac{\varepsilon_0 E_\infty}{e n_\infty}\frac{\mu_i}{\mu_e}\frac{1}{\xi^2[\xi - \eta(\xi)]}, \tag{11}$$

starting at $x(\xi_0) = 0$.

### B. Model of the main channel

The values $n_\infty$ and $E_\infty$ of the main channel, needed to solve the boundary layer equations, were determined similarly as in Ref. 7. The main channel is modeled as a non-thermal plasma cylinder of radius $R$ in which the Joule heating is balanced by the radial thermal conduction at each axial position

$$\frac{1}{r}\frac{d}{dr}\left[r\lambda\frac{dT}{dr}\right] + \eta_T \sigma E_\infty^2 + Q_{VT} = 0, \tag{12}$$

$$\frac{1}{r}\frac{d}{dr}\left[r n_{N_2} D \frac{d\varepsilon_V}{dr}\right] + \eta_V \sigma E_\infty^2 - Q_{VT} = 0, \tag{13}$$

where $T(r)$ is the gas temperature at each radial position $r$, $\varepsilon_V$ is the mean vibrational energy of nitrogen molecules, $\lambda$ is the gas thermal conductivity without the contribution from vibrational excitation of nitrogen molecules, determined from the equilibrium conductivity $\lambda_{eq}$, taken from tables,[8] as

$$\lambda = \lambda_{eq} - n_{N_2} D k_B \left(E_{N_2}/T\right)^2 \frac{\exp\left(-E_{N_2}/T\right)}{\left[\exp\left(-E_{N_2}/T\right) - 1\right]^2}, \tag{14}$$

$D$ is the diffusion coefficient of $N_2$ molecules, whose number density is $n_{N_2}$. $E_{N_2}$ is the vibrational excitation level of $N_2$ (0.29 eV) and $k_B$ is Boltzmann constant. The vibrational to translational relaxation of $N_2$ molecules is modeled through the term

$$Q_{VT} = n\frac{\varepsilon_V - \varepsilon_V(T)}{\tau_{VT}}, \tag{15}$$

with $n$ as the total number density, and where $\varepsilon_V(T)$ is the equilibrium mean vibrational energy at the gas temperature

$$\varepsilon_V(T) = \frac{E_{N_2}}{\exp\left(E_{N_2}/T\right) - 1}, \tag{16}$$

and $\tau_{VT}$ is the relaxation time.

The fraction $\eta_V$ of Joule energy going to vibrational excitation of $N_2$ is determined from the electron energy loss coefficients given by the Bolsig software as a function of the reduced electric field $E_\infty/n$. $\eta_T$ is determined in the same manner—the fraction of Joule energy that goes to the translational degrees of freedom.[8]

The electrical conductivity $\sigma$ is determined as $\sigma = e\mu_e n_e$, where the electron mobility $\mu_e$ is given as a function of the reduced electric field $E_\infty/n$.[9]

The electron number density $n_e$ is determined from the diffusion equation

$$\frac{1}{r}\frac{d}{dr}\left[rD_A\frac{dn_e}{dr}\right]+q_e=0, \tag{17}$$

in which the ambipolar diffusion coefficient $D_A$ is employed. The simplification of the model is contained in the source term $q_e$, which incorporates only the most relevant reactions in the regime considered[10,11]

$$e+NO\rightarrow e+e+NO^+, \tag{R18}$$

$$N+O\rightarrow NO^++e, \tag{R19}$$

$$NO^++e\rightarrow N+O, \tag{R20}$$

with corresponding reaction coefficients $k_{R18}$, $k_{R19}$, and $k_{R20}$, so that the source term is written as

$$q_e=k_{R18}n_en_{NO}+k_{R19}n_Nn_O-k_{R20}n_e^2, \tag{21}$$

and in which it was taken into consideration that since the gas temperature is high, there is negligible attachment,[11] so that the number density of electrons is very close to that of the positive ions $NO^+$. Also, since the degree of ionization is very low, the atomic species and $NO$ are produced mainly by collisions among heavy species, so that the densities of $N$, $O$, and $NO$ are determined from the equilibrium constants at the gas temperature

$$B_{NO}=\frac{[N][O]}{[NO]},\quad B_{N_2}=\frac{[N][N]}{[N_2]},\quad B_{O_2}=\frac{[O][O]}{[O_2]}. \tag{22}$$

In this way, by considering that $n_{N_2}+2n_N=n_{0N_2}$, with $n_{0N_2}$ the local density of $N_2$ if there were no dissociation, with an analog relation for oxygen, we obtain

$$n_N=\sqrt{B_{N_2}^2+n_{0N_2}B_{N_2}}-B_{N_2}, \tag{23}$$

$$n_O=\sqrt{B_{O_2}^2+n_{0O_2}B_{O_2}}-B_{O_2}, \tag{24}$$

$$n_{NO}=\frac{n_Nn_O}{B_{NO}}, \tag{25}$$

where the values of $n_{0N_2}$ and $n_{0O_2}$ are taken as $0.8n$ and $0.2n$, respectively. The expressions of $k_{R18}$, $k_{R19}$, $k_{R20}$, $B_{NO}$, $B_{N_2}$, and $B_{O_2}$ are taken from Ref. 7. The expressions of the diffusion coefficients and of $\tau_{VT}$ are taken from Ref. 12.

The electron temperature ($T_e$) needed in the evaluation of $D_A$ and $k_{R20}$ is obtained from the Bolsig code[13] as a function of the local reduced electric field. Vibrational temperature needed for the evaluation of $k_{R18}$ is obtained from $\varepsilon_V$ as $T_V=E_{N_2}/\ln(1+E_{N_2}/\varepsilon_V)$.

The model is closed by giving the value of $R$. The condition of zero radial derivative at $r=0$ for all magnitudes, and that $T$ and $T_V$ correspond to ambient temperature at $r=R$, while $n_e\approx 0$ at that position, allow to solve Eqs. (12), (13), and (17) with the electric field $E_\infty$ determined as the eigenvalue for which the electric current circulating in the channel

$$I=2\pi E_\infty\int_0^R\sigma(r)dr$$

takes the value corresponding to the discharge current considered.

Finally, the value of $n_\infty$ is determined as

$$n_\infty=\frac{2}{R^2}\int_0^R n_e(r)rdr. \tag{26}$$

## III. EXPERIMENTAL SETUP

The electrodes of the plasma jet system consist of two stainless steel disks of 20 mm diameter and 3 mm thickness with a center hole of 1 mm diameter. The two electrodes are attached at both sides of a dielectric disk (Teflon PTFE) with a hole at the center of 2 mm in diameter through which the air flows. Three different electrode separations $d$ can be assembled using dielectric disks of 1.3, 1.9, and 3.3 mm of thickness. The flow rate varies from 2 l/min to 16 l/min. Due to excessive heating, continuous operation is not possible with flow rates below 2 l/min. On the other hand, it is not possible to sustain the discharge with the largest electrode separation of 3.3 mm with flow rates above 8 l/min. It is for these reasons that we have chosen to present most of the results for the case of a flow rate of 8 l/min. The jet is driven by a 50 Hz commercially available transformer for neon light connected to a variable autotransformer at the maximum high voltage output of 12 kV. A schematic of the experimental setup is shown in Figure 1.

The gas flow was measured using a stainless steel float flow meter. The voltage $V$ between the electrodes was measured using a high voltage probe (Tektronix P6015A, 1000×) connected to a digital oscilloscope (Tektronix TDS2004B, 60 MHz, 1 GS/s), and the current $I$ was inferred from the voltage drop through a 100 Ω resistance (see Figure 1).

Optical emission spectra of the discharge were measured with a spectrograph HORIBA IHR320, equipped with a CCD detector. The entrance slit, of 0.2 mm width, was mounted facing the plasma jet, collecting the light emitted not only from the plasma plume but also that from the inter-electrode region. The SPECAIR software[14] was used to model the optical emission spectrum corresponding to the

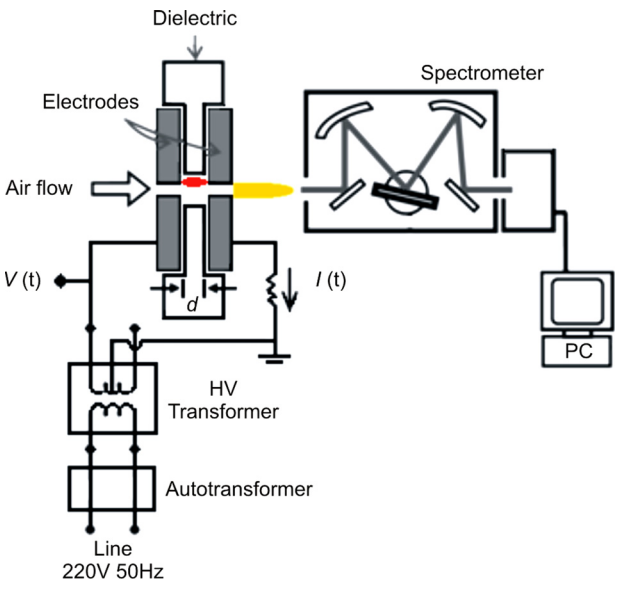


FIG. 1. Experimental device.

transitions of the $N_2$ 2nd positive system in order to determine the rotational temperature.

## IV. RESULTS

In Figure 2, a typical signal of the discharge current and voltage is shown. The current has a sinusoidal profile with a frequency of 50 Hz limited by the transformer impedance. Several current spikes appear at the beginning of each half cycle, reaching up to about 10 A amplitude, corresponding to electric breakdowns interrupted by the fast current limitation of the power source. At the end of the half cycle, when the established discharge is interrupted, another single spike appears due to inductive rising of the voltage. Each of these spikes is followed by a spurious spike of opposite sign, related to the measuring circuitry and having maximum amplitudes of about 1 A. Only after repeated, unsuccessful breakdowns does the more permanent discharge set up, probably helped by gas heating and charges left by the previous breakdowns. The voltage signal has also a frequency of 50 Hz, and as the discharge progresses, during each half cycle, the voltage decreases when the current increases and vice versa. This behavior results in a negative slope in the $V(I)$ characteristic of the discharge, which can be observed in Figure 3 for the three different electrode separations. Due to the large excursions of the electric magnitudes at the initiation and end of the discharge in each half cycle, only values of the current above 25 mA up to the maximum value (first quarter of each cycle) are used to obtain the $V(I)$ characteristics.

From the measured $V(I)$ for two different electrode separations, the main channel electric field $E_\infty(I)$, and the cathode layer voltage $\Delta V(I)$ can be determined, considering that

$$E_\infty(I) = \frac{V_i(I) - \Delta V(I)}{d_i}, \tag{27}$$

where the subscript $i$ denotes an electrode separation, and where the cathode layer thickness was neglected as compared with the electrode separation (the model predicts layer thickness of a few $\mu$m). Further assuming that $\Delta V$ is

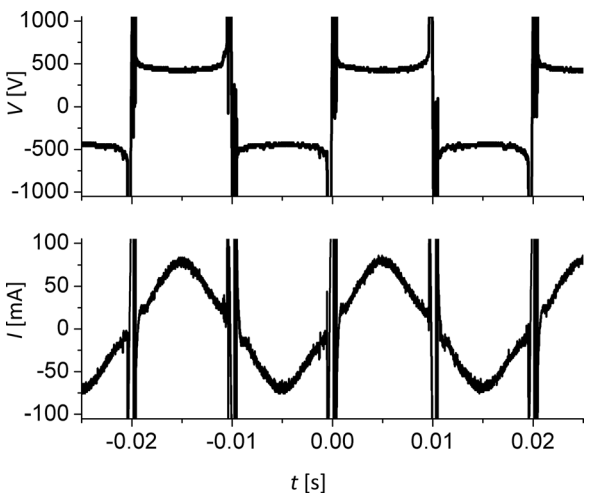


FIG. 2. Voltage and current signals of the jet for $d = 1.3$ mm and an air mass flow of 8 l/min.

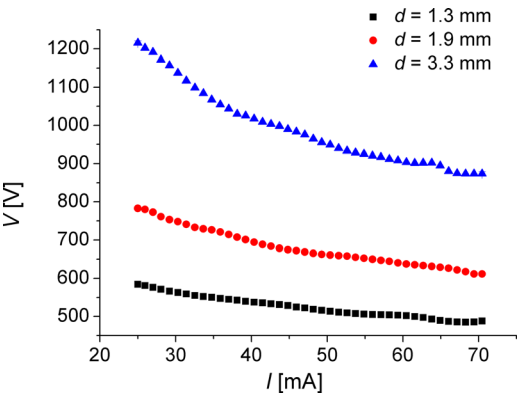


FIG. 3. Experimental $V$-$I$ characteristics for an air flow of 8 l/min with different electrode separations.

independent of $d_i$, if "1" and "2" denote two different electrode separations, one can write that

$$E_\infty(I) = \frac{V_2(I) - \Delta V(I)}{d_2} = \frac{V_1(I) - \Delta V(I)}{d_1}.$$

In this way, the cathode layer voltage can be determined as

$$\Delta V(I) = \frac{d_2 V_1(I) - d_1 V_2(I)}{d_2 - d_1}. \tag{28}$$

Figure 4 shows the experimental cathode layer voltage as a function of $I$ obtained using the separations $d = 1.3$ and 3.3 mm in expression (27), corresponding to a gas flow of 8 l/min. The error bars in this figure contain the values obtained using the other distance combinations in Eq. (27). In the same figure, the line represents the result of the cathode layer model. This result was obtained by choosing as the parameter of the model, the current dependent values of $\Phi_0$, the flow of secondary electrons emitted at the cathode due to mechanisms other than ion impact.

Also, using (28) in (27), the electric field in the main channel can be obtained as

$$E_\infty(I) = \frac{V_2(I) - V_1(I)}{d_2 - d_1}, \tag{29}$$

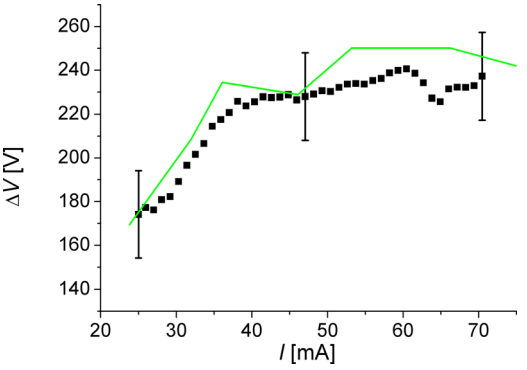


FIG. 4. Cathode-layer voltage as a function of the discharge current. Dots: experimental values corresponding to an air flow rate of 8 l/min. Line: theoretical model fit.

and it is shown in Figure 5 for $d_1 = 1.3$ and $d_2 = 3.3$ mm. The error bars in this figure contain the values obtained using the other distance combinations. The theoretical $E_\infty$ as a function of the current was obtained using the main channel model and shown in the same Figure 5 as a full line. The best accord between model and experiment was obtained for a channel radius $R$ dependent on the current, as shown in Figure 6. The corresponding gas temperature at the axis, together with the $N_2$ vibrational temperature and electron temperature at the axis, resulting from the model of the main channel, is shown in Figure 7.

In order to model the cathode layer, the secondary electron emission coefficient for the ion impact was taken as $\gamma = 0.005$, corresponding to $N_2^+$ ions.[15] Expressions of the ionization Townsend's coefficient as a function of the electric field, and of the dissociative recombination coefficient as a function of the electron temperature, were taken from Chapter 4 of Ref. 6 and from Ref. 16. In order to evaluate metastable $N_2$ contribution to the generation of secondary electrons at the cathode using Eq. (10), Townsend's coefficient for $N_2$ molecule excitation to the metastable level $N_2(A^3\Sigma_u^+)$[17] was taken as that corresponding to ionization, but corrected for the difference between ionization and excitation energies. The precise values of the metastable lifetime, which are above 1 $\mu$s,[18] are not critical because of the relatively small extensions of the cathode layer (below 10 $\mu$m, as obtained from the cathode layer model), which lead to the exponential in the integral in Eq. (10) to be very close to one. The contribution of the field-enhanced thermionic effect to the secondary electron emission was evaluated using Eq. (9) with the determined electric field at the cathode surface. In this way, for each couple of values $(n_\infty, E_\infty)$ corresponding to a given current $I$, the flow $\phi_0$ needed to match the experimental cathode layer voltage is determined, which allows to infer what should be the necessary secondary emission coefficient of metastable molecules $\gamma_m$, or the surface temperature for thermoionic emission, in order for each mechanism to sustain by itself the discharge.

It is found that the field-enhanced thermionic effect is by itself able to provide the additional flow $\phi_0$ of secondary electrons needed to sustain the discharge, for temperatures near the melting point of steel (about 1500 K), which can be justified as the gas temperature at the axis ranges between approximately 1500 and 2500 K. Additional evidence of high temperatures at the electrode surface is the damage caused by melting that can be observed after sustained operation of the discharge. On the other hand, in order to sustain the discharge with the only additional mechanism of electron emission by collision of metastable $N_2$, a corresponding secondary emission coefficient $\gamma_m > 0.08$ would be necessary. As reported values are between one and two orders of magnitude smaller,[19] it appears that this mechanism is not effective to sustain the discharge.

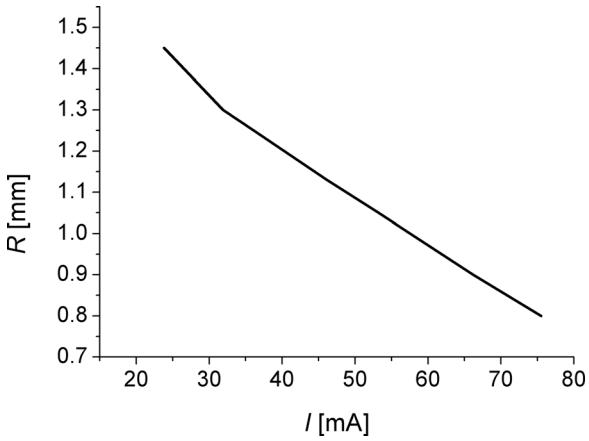


FIG. 6. Channel radius as a function of current used in the theoretical model to fit the measured electric field for a flow rate of 8 l/min.

The measured spectrum of the $N_2$ 2nd positive system (dots), together with the simulated spectrum using the SPECAIR@ software (lines), is shown in Figure 8. The simulation corresponds to $T_r = 1950$ K. Taking into consideration that the rotational temperature $T_r$ used in the simulation is a good estimator of the gas temperature $T$,[20] it can be seen that the temperature obtained from the model gives good account of the experimental spectrum.

Note that the measured spectrum around 327 nm shows a deviation from the simulated spectrum. This is due to the fact that around this wavelength, the spectrum is rather dependent on the $N_2$ vibrational temperature of the excited electronic state ($C^3\Pi$). Since the rest of the spectrum shown is not very sensitive to the precise value of the vibrational

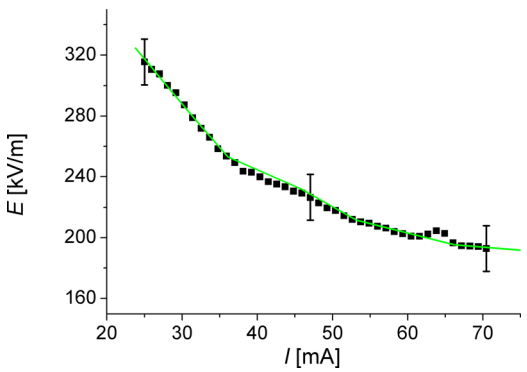


FIG. 5. Main-channel electric field as a function of the discharge current. Dots: experimental values corresponding to an air flow rate of 8 l/min. Line: theoretical model fit.

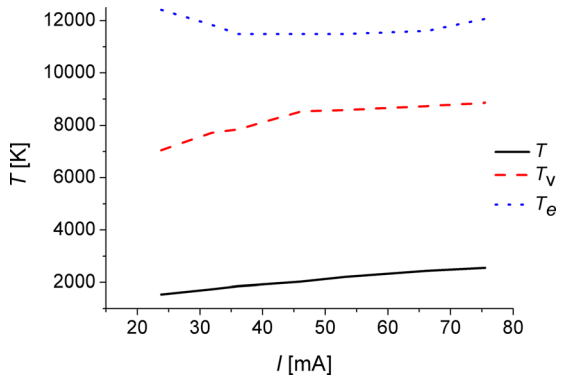


FIG. 7. Gas temperature at the axis, full line, as a function of current used in the theoretical model to fit the measured electric field for a flow rate of 8 l/min. Dashes: resulting $N_2$ vibrational temperature at the axis. Dots: resulting electron temperature at the axis.

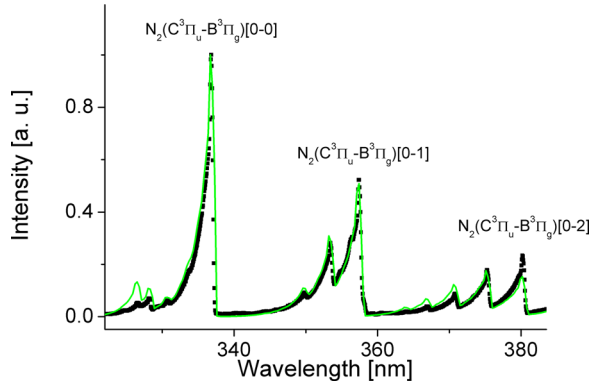


FIG. 8. Experimental spectra of the $N_2$ 2nd positive system (dots) and SPECAIR software spectral simulations (lines) corresponding to the case with an air flow of 8 l/min.

temperature but only to the rotational temperature, we have used in the SpecAir simulation the vibrational temperature provided by the model for the ground electronic state ($X^1\Sigma$), about 8000 K, which in atmospheric pressure plasmas not necessarily equals to that of the excited state.[20]

Finally, in Figure 9, the electric field in the main channel as a function of the current is shown for different air flow rates. These values were determined using expression (29) with the measured voltage and current corresponding to $d = 1.3$ and $d = 1.9$ mm, the latter being the largest separation for which the discharge can be sustained for air flows over 8 l/min. The figure shows a systematic increase in the field magnitude with the flow rate.

## V. DISCUSSION

Some worth noting results concern the obtained parameters of the cathode layer. The normal cathode fall for a glow discharge in air with a steel electrode is about 269 V, with a corresponding thickness at an atmospheric pressure (and ambient temperature) of about 7 $\mu$m.[6] The measured cathode voltages in our case are somewhat below 240 V, and as low as 180 V for the lowest currents considered, and the corresponding cathode layer thickness predicted by the cathode layer model is in the range of 5–7 $\mu$m. The cathode layer model fits the voltage measured values, also matching the

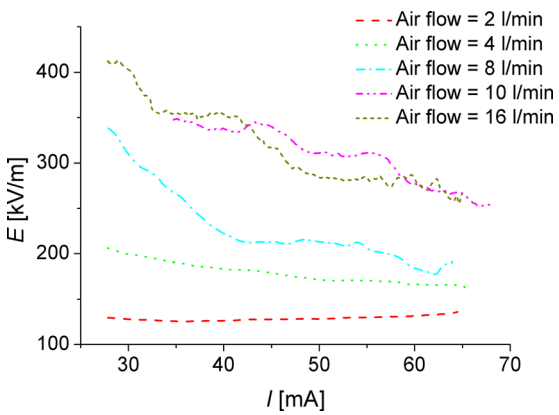


FIG. 9. Electric field in the main discharge channel as a function of the current for different air flow rates.

electric field and mean electron density in the main channel (the latter obtained from the channel model) only if an additional mechanism to that of ion collision is considered for secondary electron emission. As discussed above, the most likely additional mechanism is field-enhanced thermoionic emission, with predicted field values at the cathode surface of $4–6 \times 10^7$ V/m. The lower cathode voltages, relative to the normal cathode fall, together with the additional mechanism of secondary electron emission, indicate that the discharge is of the contracted glow type.

Another interesting result is the generation of increasingly higher values of the electric field magnitude in the main discharge channel as the gas flow increases, up to a saturation value. In order to analyze this behavior, we consider the cooling effect of the air flow on the discharge, which can be estimated by comparing the transit time of an air parcel inside the conduct with the diffusion time of the hot electrons and ions of the discharge in that parcel. For a flow rate of 10 l/min, the gas velocity is about 50 m/s, and the transit time is about 20 $\mu$s (for a 1 mm characteristic length). The characteristic time for the radial diffusion of hot electrons and ions, with an ambipolar diffusion coefficient[21] of about $5 \times 10^{-2}$ m$^2$/s and conduct radius 1 mm, is also 20 $\mu$s. In this way, below about 10 l/min, the lower the flow rate the more marked the heating of the air inside the conduct with the consequent reduction of its cooling effect on the discharge channel. The increase in the electric field as the gas flow rate increases can thus be related to the augmented cooling effect, and interpreted in terms of the corresponding augmented electrical resistivity of the channel. Since there is a maximum cooling effect obtained when the flowing gas stays close to the ambient temperature inside the conduct, one expects saturation in the thermal state of the discharge when the flow rate exceeds about 10 l/min. It is indeed at about this flow rate value that the maximum values of the electric field in the main channel are obtained, as further increasing the flow up to 16 l/min results in the same electric field magnitudes within the experimental uncertainties (see Figure 9).

In the model used, the cooling effect reflects itself in the values of the radius at which the boundary condition of the ambient temperature is enforced. For a flow of 2 l/min, the electric field and temperature of different species match those reported in similar discharges in which the influence of the gas velocity is weak.[10] As the gas flow increases, the model results in lower gas temperatures and higher vibrational temperatures, the latter directly reflecting the action of the increased electric field, and also of the smaller channel radius that reduces the time for energy exchange between vibrational and translational modes.

## VI. CONCLUSIONS

We have presented an experimental and theoretical study of a plasma-jet discharge operating with air at atmospheric pressure. Models for the cathode layer and for the main discharge channel were also employed to help understand the physical mechanisms involved, in particular, the novel characteristic of generation of large values of the electric field in the plasma channel, needed to sustain the discharge against

strong cooling by the gas flow, which at the highest flow rates results in air transit times of the same order of the kinetic diffusion times in the conduct. These high values of the electric field can be useful to generate a substantial number of high energy electrons capable of high-threshold energy reactions if, for instance, small mixtures of additional gas components are added to the incoming gas flow.

Also, the model of the main channel employed is useful to derive detailed information of the plasma state from relatively simple electrical measurements, allowing, for instance, to determine reactive species production, temperatures, etc.

## ACKNOWLEDGMENTS

This work was financed by grants from CONICET: PIP GI 11220120100453 and from the University of Buenos Aires: UBACyT 20020150100096BA.

[1]D. B. Graves, Phys. Plasmas. **21**, 080901 (2014).
[2]M. G. Kong, G. Morfill, and W. Stolz, in *Plasma Medicine*, edited by M. Laroussi (Cambridge University Press, Cambridge, 2012).
[3]X. Lu, G. V. Naidis, M. Laroussi, S. Reuter, D. B. Graves, and K. Ostrikov, Phys. Rep. **630**, 1–84 (2016).
[4]F. Minotti, L. Giuliani, M. Xaubet, and D. Grondona, Phys. Plasmas **22**, 113512 (2015).
[5]E. L. Murphy and R. H. Good, Phys. Rev. **102**, 1464 (1956).
[6]Y. P. Raizer, in *Gas discharge physics*, edited by J. E. Allen (Springer Verlag, Berlin, 1991) pp. 68–71, 277, 327.
[7]M. S. Benilov and G. V. Naidis, J. Phys. D: Appl. Phys. **36**, 1834–1841 (2003).
[8]M. I. Boulos, P. Fauchais, and E. Pfender, *Thermal Plasmas: Fundamentals and Applications* (Plenum Press, New York, 1994), Vol. 1, pp. 314–317.
[9]R. Morrow and J. J. Lowke, J. Phys. D: Appl. Phys. **30**, 614–627 (1997).
[10]G. V. Naidis, Plasma Sources Sci. Technol. **16**, 297–303 (2007).
[11]L. Prevosto, H. Kelly, B. Mancinelli, J. C. Chamorro, and E. Cejas, Phys. Plasmas **22**, 023504 (2015).
[12]J. A. Riousset, V. P. Pasko, and A. Bourdon, J. Geophys. Res. **115**, A12321, doi:10.1029/2010JA015918 (2010).
[13]G. J. M. Hagelaar and L. C. Pitchford, Plasma Sources Sci. Technol. **14**, 722–733 (2005).
[14]See http://www.specair-radiation.net/ for Specair program characteristics; accessed October 2016.
[15]V. A. Lisovskiy, N. D. Kharchenko, and V. D. Yegorenkov, J. Phys. D: Appl. Phys. **43**, 425202 (2010).
[16]P. Lukáč, O. Mikuš, I. Morva, Z. Zábudlá, J. Trnovec, and M. Morvová, Plasma Sources Sci. Technol. **20**, 055012 (2011).
[17]See http://www.nist.gov/pml/data/asd.cfm for NIST atomic database.
[18]D. E. Shemansky, J. Chem. Phys. **51**, 5487–5494 (1969).
[19]P. Strake, F. Wiegershaus, S. Krischok, and V. Kempter, Surf. Sci. **396**, 212–220 (1998).
[20]D. Staack, B. Farouk, A. F. Gutsol, and A. A. Fridman, Plasma Sources Sci. Technol. **15**, 818–827 (2006).
[21]M. Capitelli, C. M. Ferreira, B. F. Gordiets, and A. I. Osipov, *Plasma Kinetics in Atmospheric Gases* (Springer, 2000), pp. 95–99.